

Nanoscale

Accepted Manuscript



This is an *Accepted Manuscript*, which has been through the Royal Society of Chemistry peer review process and has been accepted for publication.

Accepted Manuscripts are published online shortly after acceptance, before technical editing, formatting and proof reading. Using this free service, authors can make their results available to the community, in citable form, before we publish the edited article. We will replace this *Accepted Manuscript* with the edited and formatted *Advance Article* as soon as it is available.

You can find more information about *Accepted Manuscripts* in the [Information for Authors](#).

Please note that technical editing may introduce minor changes to the text and/or graphics, which may alter content. The journal's standard [Terms & Conditions](#) and the [Ethical guidelines](#) still apply. In no event shall the Royal Society of Chemistry be held responsible for any errors or omissions in this *Accepted Manuscript* or any consequences arising from the use of any information it contains.



Large area chemical vapor deposition of monolayer transition metal dichalcogenides and their temperature dependent Raman Spectroscopy studies

Received 00th January 20xx,
Accepted 00th January 20xx

DOI: 10.1039/x0xx00000x

www.rsc.org/

Amit S. Pawbake,^{a,b} Mahendra S. Pawar,^a Sandesh R. Jadkar,^b Dattatray J. Late^{a*}

We investigate the growth mechanism and temperature dependent Raman spectroscopy of chemically vapor deposited large area monolayer of MoS₂, MoSe₂, WS₂ and WSe₂ nanosheets up to 70 μm in lateral size. Further, our temperature dependent Raman spectroscopy investigation shows that softening of Raman modes as temperature increases from 80K to 593K due to the negative temperature coefficient and anharmonicity. The temperature dependent softening modes of chemically vapor deposited monolayers of all TMDCs were explained on the basis of a double resonance phonon process which is more active in an atomically thin sample. This process can also be fundamentally pertinent in other emerging two-dimensional layered and heterostructured materials.

Introduction

The atomically thin transition metal dichalcogenides (TMDCs)¹⁻⁶ materials such as MoS₂, MoSe₂, WS₂, WSe₂, MoTe₂ etc have been gained much interest due to their prospective applications in nanoelectronics and optoelectronics devices.¹⁻⁸ For example, the bulk MoS₂ is semiconducting in nature and possesses indirect band gap of 1.2 eV and while the monolayer has direct and wide band gap of 1.8 eV⁹. Similarly the monolayers of MoSe₂, WS₂, and WSe₂ possesses direct band gap of 1.58 eV,¹⁰ 2.1 eV,¹¹ and 1.6 eV¹²

respectively. The tuning of bandgap from monolayer to bulk affects the various properties such as electrical, optical, chemical, magnetic, mechanical properties which indeed show its potential applications in various nanoelectronics and optoelectronic devices. Recently chemical vapor deposition (CVD) method has been widely used to deposit the nanosheets of various inorganic and other emerging materials due to fast, large area and control growth of the materials.¹³⁻¹⁴ The sample prepared under identical conditions by various research groups shows that the variation in the mobility is due to the poor quality of the sample.¹⁵⁻¹⁶ It is important to understand the vibrational properties of these chalcogenides layered materials prepared in the identical condition and instrument.¹⁷

^{a,*} Physical and Material Chemistry Division, CSIR – National Chemical Laboratory, Pune, 411008, Maharashtra, India. E-mail: datta099@gmail.com; dj.late@ncl.res.in

^b School of Energy Studies, Department of Physics, Savitribai Phule Pune University, Pune 411007, India.

Raman spectroscopy is very appropriate and advanced technique to characterize the structural, optical and mechanical properties of layered material such as graphene,¹⁸⁻²⁴ MoS₂,²⁵⁻²⁸ MoSe₂,²⁸⁻³⁰ WS₂,^{24,31-32} WSe₂,^{28,29,33} MoTe₂,³⁴ WTe₂,³⁵ Black phosphorous,³⁶ TiS₃³⁷ and other layered materials³⁸. The Raman spectroscopy technique is widely used to identify the number of layers present in the graphene by monitoring 2D bands position and intensity ratio, as well used to find out diameter of single walled carbon nanotubes (SWNT's)³⁹⁻⁴³ and number of layers present in the 2D chalcogenide¹⁶⁻²⁶. The investigations of the vibrational properties of chalcogenides layered materials is important to know electron-phonon interaction, which plays a significant role on the electronic behavior of the nanodevices and thus it can even affects the charge carrier mobility,^{2,44}. The systematic study of the vibrational properties of CVD grown MoS₂, WS₂, WSe₂ and MoSe₂ at wide temperature range is still lacking in the literature. The Raman spectra of MoS₂ shows strong out-of plane mode and in-plane mode as an prominent peaks corresponding to the excitation of (E_{2g}¹) and (A_{1g}) Raman modes, whose frequencies exhibit a linear temperature dependence over the entire temperature range from 80 K to 593 K. The first order temperature coefficients (χ) associated with each Raman mode has been calculated from the slope of straight line fitted with Raman shift as a function of temperature.^{23, 45} This observed variation with temperature in Raman mode, is similar to that observed in other 2D systems including graphene.⁴⁶⁻⁴⁸

We present here the CVD grown monolayer MoS₂, MoSe₂, WS₂ and WSe₂ under argon (Ar) atmosphere without using vacuum and present its temperature dependent Raman spectroscopy studies.

Experimental Methods:

Synthesis Method

Chemical vapor deposition of single-layer MoS₂:

We have synthesized monolayer MoS₂ by using CVD method containing two heating zones (as shown in supporting Information figure S1 (a)). In typical experiment, Sulfur (S) powder (99.9%, Sigma Aldrich) was placed in the first zone at upstream, and Molybdenum Oxide (MoO₃) powder (99.5%, HPLC analytic reagent grade) was placed inside the quartz tube (50 mm dia.) in the second zone. A cleaned 300 nm SiO₂/Si wafers were then placed face down on the alumina boat which contains MoO₃ powder. The temperature of second zone was raised up to 750 °C with a heating ramp of 10°C/min and the deposition was taken at 750°C for 10 min. During the same time, the temperature of the first zone was also reached at 120°C so as to evaporate the sulfur powder. After the deposition furnace was allowed to cool naturally to room temperature. During all the growth process, the argon flow rate was maintained at 50 SCCM.

Chemical vapor deposition of single-layer MoSe₂:

In typical experiment, Selenium (Se) powder (99.9%, Sigma Aldrich) was placed in the first zone at upstream, and MoO₃ powder was placed inside the quartz tube (50 mm dia.) in the second zone. A cleaned 300 nm SiO₂/Si wafers were then placed face down on the alumina boat which contains MoO₃ powder. The temperature of second zone was raised up to 750°C with a heating ramp of 10°C/min and the deposition was taken at 750°C for 10 min. Further, the temperature of the first zone was also reached at 250°C so as to evaporate the Se powder on same time of reaction. After the reaction furnace was allowed to cool naturally to room temperature. During all the growth process flow rate of gas was maintained at 50 SCCM (Ar 40 SCCM + 10 SCCM H₂).

Chemical vapor deposition of single-layer WS₂:

In typical experiment, S powder was placed in the first zone of furnace at upstream and Tungsten Oxide (WO_3) powder (99.5%, HPLC analytic reagent grade) was placed inside the quartz tube (50 mm dia.) in the second zone. A cleaned 300 nm SiO_2/Si wafers were then placed face down on the alumina boat which contains WO_3 powder. The temperature of second zone was raised up to 950 °C with a heating ramp of 10°C/min and the deposition was taken at 950°C for 10 min. The care has been taken so as to reach the temperature of the first zone at 120°C on same time of reaction so as to evaporate the S powder. After the deposition furnace were allowed to cool down naturally to room temperature. During all the growth process, the Ar gas flow rate was maintained at 50 SCCM.

Chemical vapor deposition of single-layer WSe_2 :

In typical experiment, Se powder was placed in the first zone at upstream and WO_3 powder was placed inside the quartz tube (50 mm dia.) in the second zone. A cleaned 300 nm SiO_2/Si wafers were then placed face down on the alumina boat which contains WO_3 powder. The temperature of second zone was raised up to 950 °C with a heating ramp of 10°C/min and the reaction were carried out at 950°C for 10 min. The temperature of the first zone was raised upto 250°C so as to evaporate the Se powder on the same time of reaction. After the deposition the furnace was allowed to cool down naturally to room temperature. During all the growth process gas flow rate was maintained at 50 SCCM (Ar 40 SCCM +10 SCCM H_2).

Material Characterizations

Chemical vapor deposited monolayer of MoS_2 , MoSe_2 , WS_2 , and WSe_2 were characterized using Optical microscope, atomic force microscopy (AFM) and Raman spectroscopy. The temperature dependent Raman spectroscopy of all TMDCs were carried out using Renishaw InVia microscope Raman system with laser wavelength 532 nm in the back scattering geometry. The detector

used was CCD synapse with thermoelectric cooling to -70°C. A 50X objective was used to focus the laser beam and to collect the Raman signal. The laser power on the sample was ~5 mW with laser spot size ~1 μm to avoid the possible heating effect by the laser on the monolayer samples. The peak positions, intensity and line widths were extracted by fitting the experimental data with Lorentzian functions. The Optical images were captured using Nikon Eclipse LV 150 NL optical microscope. Auto exposure times were used during the image recording, which can be varied in the range of 10-500 ms. The AFM images were acquired using Bruker's multi code 8 instrument with tapping mode.

Results and Discussion

Growth mechanism of single-layer TMDCs and morphology analysis

In present investigations, we have synthesized monolayer TMDCs by simple vapor solid mechanism using tubular furnace. Figure S2 (a-b) shows the typical side view and top view of monolayer TMDC's. The formation of triangular shape of TMDCs nanosheets and its growth mechanism is completely depends on four factors such as (i) gas flow rate, (ii) substrate temperature, (iii) substrate which also plays an important role, and finally (iv) the ratio of M: X powder (where M: Mo, W and X: Se, S etc). Figure 1 (a) shows a typical optical image of triangular shape single layer MoS_2 nanosheet with typical lateral dimension of ~ 35 μm . The single-layer and few layer natures of MoS_2 and other TMDCs sample were identified by using specific color contrast of layers using optical microscope^{49, 50}. Further AFM image and AFM height profile were measured so as to confirm the number of layers present in the sample. Additionally, the Raman spectrum was analyzed to identify number of layers present in the MoS_2 nanosheet sample. Figure 1(b)

shows the typical Raman spectrum for single layer MoS₂ recorded at room temperature. Typical Raman spectrum of single-layer MoS₂ consist of two modes E_{2g}¹ and A_{1g} arises due to the in plane and out of plane mode. The in plane mode consist of vibration of two S atom in one direction and Mo atom in opposite direction. While in case of out of plane mode two S atoms vibrate opposite to each other while Mo atom remains stable⁵¹. The peak frequency difference can also be monitored to find out the number of layers present in the sample. In present case, the Raman frequency difference of E_{2g}¹ and A_{1g} ~19.5 cm⁻¹ were observed which indicates single layer nature of MoS₂ nanosheets sample.^{51, 52} Figure 1(c) shows a typical AFM image of single-layer MoS₂ and figure 1(d) shows typical AFM height profile which shows the thickness of nanosheets ~ 0.8 nm which confirms the single layer nature of MoS₂. Figure 1 (e-f) shows typical optical images of MoS₂ synthesized >750°C which shows stacking of layers. Figure 2 (a) shows a typical optical image of triangular shape single layer MoSe₂ with lateral dimension ~ 60 μm. Figure 2(b) shows the typical Raman spectrum of single layer MoSe₂ recorded at room temperature. The most prominent peak A_{1g} is observed at 240 cm⁻¹ due to out of plane vibration which undergoes softening of A_{1g} mode in monolayer due to decreasing inter-planar restoring force.^{52, 29} Figure 2(c) shows a typical AFM image of single-layer MoSe₂ nanosheet sample and figure 2(d) shows typical AFM height profile with observed thickness of sample ~ 1.1 nm which confirms the single layer nature of MoSe₂ nanosheet sample. Figure 2 (e-f) shows typical optical images of MoSe₂ synthesized >750°C which shows stacking of layers. The evolution of interlayer coupling originates from the repulsive steric effects⁵³ that lead to different interlayer separations between the two MoS₂ layers in different stacking configurations as seen in the optical image Figure 1 (e-f). According

to steric effect, each atom acquires a certain amount of space that strongly repel with each other due to a significant energy from overlapping of electron clouds. The strong repulsion between two S atoms of the two different layers occurs when the S atom of the top layer sits on the S atom of the bottom layer in an eclipsed fashion at the interlayer distance. The atomic size and interlayer distance are the key parameters for observing steric effect in layered materials.^{53, 54}

Figure 3(a) shows a typical optical image for single layer WS₂ with lateral dimension of ~ 15μm. Figure 3(b) shows typical Raman spectrum of single layer WS₂ recorded at room temperature which consists of E_{2g}¹ first order mode at 356.6 cm⁻¹ the Brillouin zone center and A_{1g} zone edge mode at 420 cm⁻¹ which has been observed as a longitudinal acoustic mode i.e. LA (M) at the M point.^{31, 55} The LA (M) mode at 175 cm⁻¹ arises due to M-point phonon which refers to particular direction and magnitude q of the phonon.^{31, 55} The other peaks in the spectrum arise due to multiphonon combinations of first order mode, zone edge mode and longitudinal acoustic modes.^{31, 56-57} It is well known that intensity of 2LA (M) peak increases with the decreasing number of layers and there is softening of A_{1g} mode due to the decreasing restoring force and fine stiffening of 2LA (M) and E_{2g}¹ (Γ) modes accordant with the increasing restoring force arises due to the Van der Waals interactions between the layers.⁵⁷ Figure 3(c) shows a typical AFM image of single-layer WS₂ nanosheet sample and figure 3(d) shows the corresponding AFM height profile depicting thickness of sample ~ 1 nm which confirms the single layer nature of WS₂ nanosheet. Figure 3 (e-f) shows typical optical image of WS₂ nanosheet synthesized >950°C showing few layer thick nature of hexagonal shape nanosheets sample along with monolayer triangles are also seen. Figure 4(a) shows a typical optical image of single layer WSe₂

with lateral dimension observed to be 30-60 μm . Figure 4(b) shows the typical Raman spectrum of single layer WSe_2 recorded at room temperature depicting the first order peak E_{2g}^1 arises at 247 cm^{-1} due to Brillouin zone center and zone edge phonons, the second order peak 2LA(M) observed due to longitudinal acoustic phonons at the M-point in the Brillouin zone.^{51, 29, 58-59} Figure 4(c) shows a typical AFM image of single-layer WSe_2 nanosheets synthesized under identical environment and figure 4(d) shows the corresponding AFM height profile with thickness 1.1 nm which indicates the single layer nature of WSe_2 nanosheets sample. Figure 4 (e-f) shows typical optical image of WSe_2 nanosheets synthesized $> 950^\circ\text{C}$ showing few layer thick hexagonal shape nanosheets sample along with monolayer triangles are also seen.

It is observed that if the growth temperature is ($> 750^\circ\text{C}$) for case of MoS_2 and MoSe_2 the monolayer along with bilayer sheets were also formed for 10 min of reaction time, which is shown in figure 1 (e-f) and figure 2 (e-f) respectively. For temperature $\sim 750^\circ\text{C}$ we observed monolayer MoS_2 and MoSe_2 which were shown in figure 1(a) and figure 2(a) respectively for 10 min of reaction time. In case of WS_2 and WSe_2 we observed few layer hexagonal shape along with monolayer triangles at the temperature ($> 950^\circ\text{C}$) for 10 min of reaction time, which is shown in figure 3 (e-f) and figure 4 (e-f) respectively. While monolayer triangular shape of WS_2 and WSe_2 were observed for the reaction carried out at temperature ($\sim 950^\circ\text{C}$) for 10 min as seen from optical images shown in figure 3(a) and 4(a). *Bilu Liu et.al*⁶⁰ reported that in case of monolayer WSe_2 shape evolution completely depends on substrate temperature. It is also observed that lateral size of triangles are more on insulating substrates such as (SiO_2 and quartz) as compared to conducting substrates such as *p*-Si and *n*-Si (See supporting information figure S3 for optical images). *Shanshan Wang et.al*⁶¹ reported that, if

Mo:S ratio is $> 1:2$ then it forms triangular shape nanosheet with Mo terminate boundary. The majority of monolayer sample are well aligned with the relative orientation of edges that can be termed as multiples of 60° which can be confirmed by measuring the area of equilateral triangle⁶¹. If Mo:S ratio is equal to 1:2 then hexagonal shape of monolayer with Mo and S terminate boundary were formed. If Mo:S ratio is less than 1:2 then triangular shape of TMDC monolayer were formed.⁶¹

Temperature dependent Raman spectroscopy of TMDCs

Figure S1 (b) shows typical experimental set-up used to carry out the temperature dependent Raman spectroscopy studies of monolayer TMDC's. Figure 5(a) and (b) represents the typical Raman shift versus temperature plot for the CVD grown monolayer MoS_2 and MoSe_2 nanosheet sample respectively. From the plot it is clearly seen that there is downshift in the Raman modes with the increasing temperature. Further, with increasing temperature an increase in the full width at half maximum (FWHM) of the peak were observed for all the monolayer TMDCs. Figure 5 (c) and (d) shows the typical plot for the Raman shift as a function of temperature for the CVD grown WS_2 and WSe_2 nanosheet sample respectively. The plot clearly shows the downshift in the Raman modes with the increasing temperature. Apparently, the temperature dependence of the Raman spectrum of all these chalcogenides nanosheets is similar to graphene.^{46, 48} Figure 6 (a-f) shows the typical plot for Raman spectra peak position as a function of temperature for the monolayer MoS_2 , WS_2 , MoSe_2 , and WSe_2 sample respectively. The possible vibrational modes seen in TMDCs are shown in supporting information figure S4. The Raman modes for MoS_2 , WS_2 , MoSe_2 , and WSe_2 behave linearly with the temperature range from 80K to 593K. The Raman peak positions

were calculated by fitting the Lorentzian functions for each mode as function of temperature given by the equation (1),⁶²

$$\omega(T) = \omega_0 + \chi T \quad \dots (1)$$

Where, ω_0 is the peak position of A_{1g} , E_{2g}^1 and B_{2g} vibration modes at zero Kelvin temperature, χ be the first order temperature coefficient of the A_{1g} , E_{2g}^1 and B_{2g} mode. The Raman modes A_{1g} , E_{2g}^1 and B_{2g} behave straight line with temperature and the slope of the fitted straight line gives the temperature coefficient (χ). The calculated values for temperature coefficients and change in Raman frequency as a function of temperature for different modes are shown in table 1. The change in the Raman modes with the temperature is mostly due to the contribution from the thermal anharmonicity i.e. from thermal expansion and volume contribution. The Raman phonon frequency ω as a function of temperature and volume is as shown below,⁶³

$$\left(\frac{\partial \ln \omega}{\partial T}\right) P = \left(\frac{\partial \ln V}{\partial T}\right) P \left(\frac{\partial \ln \omega}{\partial \ln V}\right) T + \left(\frac{\partial \ln \omega}{\partial T}\right) V$$

$$\left(\frac{\partial \ln \omega}{\partial T}\right) P = -\frac{\gamma}{k} \left(\frac{\partial \ln \omega}{\partial P}\right) T + \left(\frac{\partial \ln \omega}{\partial T}\right) V \quad \dots (2)$$

Where, $\gamma \approx (\partial \ln V / \partial T) P$ and $k \approx -(\partial \ln V / \partial P) T$ be the volume thermal coefficient and isothermal volume compressibility. The first term from the right hand side of the equation (2) gives the volume contribution at constant temperature and second term represents the temperature contribution at constant volume. The anharmonic contribution can be calculated from the values of isobaric temperature, isothermal pressure derivative of phonon frequencies of the modes, γ , κ . The change in the FWHM, intensity and shift in the peak position as a function of temperature can be explained by using double resonance phenomenon which is very active in single layer sample. The broadening in the Raman modes with the temperature is based on the phonon dispersion and many body

theoretical calculations. The change in the FWHM is mainly due to the contribution from the decay of zone center optical phonon into one acoustic and one optical phonon and these two phonons were selected from the phonon density states of all the TMDC's. The change in the line width as a function of temperature is given by the equation,⁶⁴

$$\Gamma(T) = \Gamma_0 + A [1 + n(\omega_1, T) + n(\omega_2, T)] \quad \dots (3)$$

Where, Γ_0 represents the background contribution, A is the anharmonic coefficient and $n(\omega, T)$ is the Bose-Einstein contribution function. The temperature dependent FWHM can be determined from the parameters such as Γ_0 , A , ω_1 and ω_2 . The change in the Raman frequency ($\Delta\omega$) for the Raman modes E_{2g}^1 , A_{1g} , in monolayer MoS_2 was found to be 8 and 6.11 cm^{-1} respectively also for A_{1g} in MoSe_2 it was 4.75, in case of WS_2 for E_{2g}^1 and A_{1g} the calculated values were 4.51 and 6.43 cm^{-1} . The change in the Raman frequency for the Raman modes A_{1g} in monolayer WSe_2 was found to be 3.81 cm^{-1} .

Conclusion

In conclusion, we have systematically reported the CVD growth of large area single layer MoS_2 , MoSe_2 , WS_2 and WSe_2 and studied its temperature dependent Raman spectroscopy. We have extracted the values of temperature coefficient and observed the change in Raman peak position with varying temperature for monolayer TMDC's. The shifts in the Raman spectra of TMDCs were mainly contributed from the thermal and an anharmonic property. The softening of all the Raman modes were further explained in terms of double resonance phenomenon which is very active in single layer sample. The temperature dependent Raman spectroscopy method can also be applicable in monitoring the device

performance and other emerging properties of various other layered materials.

Acknowledgements

Dr. D. J. Late would like to thank Prof. C. N. R. Rao (FRS), JNCASR and ICMS Bangalore (India) for encouragement and support. The research work was supported by Department of Science and Technology (Government of India) under Ramanujan Fellowship to Dr. D. J. Late (Grant No. SR/S2/RJN-130/2012), NCL-MLP project grant 028626, DST-SERB Fast-track Young scientist project Grant No. SB/FT/CS-116/2013, Broad of Research in Nuclear Sciences (BRNS Grant No. 34/14/20/2015 (Government of India), partial support by INUP IITB project sponsored by DeitY, MCIT, Government of India. Authors would like to thank Director, CSIR-National Chemical Laboratory for the experimental facilities.

Notes and References

- [1] K. S. Novoselov, D. Jiang, F. Schedin, T. J. Booth, V. V. Khotkevich, S.V. Morozov and A. K. Geim, *Proc. Nat. Acad. Sci.*, 2005, **102**, 10451–10453.
- [2] Q. H. Wang, K. Kolantar-Zadeh, A. Kis, J. N. Coleman and M. S. Strano, *Nat. Nano*, 2012, **7**, 699-712.
- [3] B. Liu, M. Kopf, A. A. Abbas, X. Wang, Q. Guo, Y. Jia, F. Xia, R. Wehrich, F. Bachhuber, F. Pielnhofner, H. Wang, R. Dhall, S. B. Cronin, M. Ge, X. Fang, T. Nilges and C. Zhou. *Adv. Mater.*, 2015, **27**, 4423– 4429.
- [4] B. Liu, L. Chen, G. Liu, A. N. Abbas, M. Fathi, and C. Zhou. *ACS Nano*, 2014, **8**, 5304-5314.
- [5] L. Chen, B. Liu, A. N. Abbas, Y. Ma, X. Fang, Y. Liu, and C. Zhou. *ACS Nano*, 2014, **8**, 11543-11551.
- [6] L. Chen, B. Liu, M. Ge, Y. Ma, A. N. Abbas, and C. Zhou. *ACS Nano*, 2015, **9**, 8368-8375.
- [7] D. J. Late, B. Liu, H. R. Matte, V. P. Dravid and C. N. R. Rao, *ACS Nano*, 2012, **6**, 5635-5641.
- [8] D. J. Late, Y. K. Huang, B. Liu, J. Acharya, S. N. Shirodkar, J. Luo, A. Yan, D. Charles, U. V. Waghmare, V. P. Dravid and C. N. R. Rao, *ACS Nano*, 2013, **7**, 4879-4891.
- [9] K. F. Mak, C. Lee, J. Hone, J. Shan and T. F. Heinz, *Phys. Rev. Lett.*, 2010, **105**, 136805.
- [10] Y. Zhang, T-R Chang, B. Zhou, Y.-T. Cui, H. Yan, Z.Liu, F. Schmitt, J. Lee, R. Moore, Y. Chen, H. Lin, H.-T. Jeng, S.-K. Mo, Z. Hussain, A. Bansil and Z-X Shen. *Nat. Nanotechnol.*, 2014, **9**, 111–115.
- [11] T. Georgiou, R. Jalil, B.D. Belle, L. Britnell, R. V. Gorbachev, S. V. Morozov, Y-J Kim, A. Gholinia, S. J. Haigh, O. Makarovskiy, L. Eaves, L. A. Ponomarenko, A.K. Geim, K.S. Novoselov and A. Mishchenko. *Nat. Nanotechnol.*, 2013, **8**, 100–103.
- [12] W. Liu, J. Kang, D. Sarkar, Y. Khatami, D. Jena, and K. Banerjee. *Nano lett.*, 2013, **13**, 1983-1990.
- [13] G. He, K. Ghosh, U. Singiseti, H. Ramamoorthy, R. Somphonsane, G. Bohra, M. Matsunaga, A. Higuchi, N. Aoki, S. Najmaei, Y. Gong, X. Zhang, R. Vajtai, P. M. Ajayan, and J. P. Bird. *Nano lett.*, 2015, **15**, 5052-5058.
- [14] Y. Ma, B. Liu, A. Zhang, L. Chen, M. Fathi, C. Shen, A. N. Abbas, M. Ge, M. Mecklenburg, and C. Zhou. *ACS Nano*, 2015, **9**, 7383-7391.
- [15] Y. Zhang, Y. Zhang, Q. Ji, J. Ju, H. Yuan, J. Shi, T. Gao, D. Ma, M. Liu, Y. Chen, X. Song, H. Y. Hwang, Y. Cui and Z. Liu, *ACS Nano*, 2013, **7**, 8963–8971.

- [16] Y.-H. Lee, L. Yu, H. Wang, W. Fang, X. Ling, Y. Shi, C.-T. Lin, J.-K. Huang, M.-T. Chang, C.-S. Chang, M. Dresselhaus, T. Palacios, L.-J. Li and J. Kong, *Nano Lett.*, 2013, **13**, 1852–1857.
- [17] Q. Ji, Y. Zhang, Y. Zhang, and Z. Liu. *Chem. Soc. Rev.*, 2015, **44**, 2587-2602.
- [18] N. Bonini, M. Lazzeri, N. Marzari and F. Mauri, *Phys. Rev. Lett.*, 2007, **99**, 176802-176805.
- [19] A. C. Ferrari, J.C. Meyer, V. Scardaci, C. Casiraghi, M. Lazzeri, F. Mauri, D. Piscanec, S. Jiang, K. S. Novoselov, S. Roth and A. K. Geim, *Phys. Rev. Lett.*, 2006, **97**, 187401-107404.
- [20] L. M. Malard, M. A.Pimenta, G. Dresselhaus and M. S. Dresselhaus, *Physics Reports*, 2009, **473**, 51-87.
- [21] I. Calizo, F. Miao, W. Bao, C. N. Lau and A. A. Balandin, *Appl. Phys. Lett.*, 2007, **91**, 071913-071915.
- [22] A. Gupta, G. Chen, P. Joshi, S. Tadigadapa and P. C. Eklund, *Nano Lett.*, 2006, **6**, 2667-2673.
- [23] I. Calizo, A. A. Balandin, W. Bao, F. Miao and C. N. Lau, *Nano Lett.*, 2007, **7**, 2645-2649.
- [24] R. Narula and S. Reich, *Phys. Rev. B*, 2008, **78**, 165422-165427.
- [25] Y. Wang, C. Cong, C. Qiu and T. Yu, *Small*, 2013, **9**, 2857-2861.
- [26] R. Yan, J. R. Simpson, S. Bertolazzi, J. Brivio, M. Watson, X. Wu, A. Kis, T. Luo, A. R. H. Walker and H. G. Xing, *ACS Nano*, 2014, **8**, 986-993.
- [27] M. Thripuranthaka, R. V. Kashid, C. S. Rout and D. J. Late, *Appl. Phys. Lett.*, 2014, **104**, 081911-081915.
- [28] P. Tanndorf, R. Schmidt, P. Bottger, X. Zhang, J. Borner, A. Lietrig, M. Albretch, C. Kloc, O. Gordan, D. R. T. Zahn, S. M. de. Vasconcellos and R. Bratschitsch, *Optics Express*, 2013, **21**, 4908-4916.
- [29] D. J. Late, S. N. Shirodkar, U. V. Waghmare, V. P. Dravid and C.N. R. Rao, *Chem. Phys. chem.*, 2014, **15**, 1592 – 1598.
- [30] D. J. Late, T. Doneux and M. Bougouma, *Appl. Phys. Lett.*, 2014, **105**, 233103.
- [31] A. Berkdemir, H. R. Gutierrez, A. R. Bontello-Mendez, N. Perea-Lopez, A. L. Elias, C-I. Chia, B. Wang, V. H. Crespi, F. Lopez-Urias, J-C. Charlier, H. Terrones and M. Terrones, *Sci. Rep.*, 2013, **3**, 1755-1762.
- [32] M.Thripuranthaka, D. J. Late, *ACS Appl. Mater. Interfaces*, 2014, **6**, 1158-1163.
- [33] X. Luo, Y. Zhao, M. Toh, C. Kloc, Q. Xiong and S. Y. Quek, *Phys. Rev. B*, 2013, **88**, 195313- 195319.
- [34] M. Yamamoto, S. T. Wang, M. Ni, Y. F. Lin, S. L. Li, S. Aikawa, W. B. Jian, K. Ueno, K. Wakabayashi and K. Tsukagoshi, *ACS Nano*, 2014, **8**, 3895–3903.
- [35] M. K. Jana, A. Singh, D. J. Late, C. Rajamathi, K. Biswas, C. Felser, U. V. Waghmare and C. N. R. Rao, *J. Phys.: Condens. Matter.*, 2015, **27**, 285401.
- [36] M. Buscema, D. J. Groenendijk, S. I. Blanter, G. A. Steele, H. SJ van der Zant, and A. Castellanos-Gomez. *Nano lett.*, 2014, **14**, 3347-3352.
- [37] A. S. Pawbake, J. O. Island, E. Flores, J. R. Ares, C. Sanchez, I. J. Ferrer, S. R. Jadkar, H. S. vander Zant, A. Castellanos-Gomez, and D. J Late, *ACS Appl. Mater. Interfaces*. 2015, **7**, 24185–24190.
- [38] D. J. Late, B. Liu, J. Luo, A. Yan, H. S. S. R. Matte, M. Grayson, C. N. R. Rao and V. P. Dravid, *Adv. Mater.*, 2012, **24**, 3549-3554.

- [39] P. V. Huong, R. Cavagnat, P. M. Ajayan and O. Stephan, *Phys. Rev. B*, 1995, **51**, 10048-10051.
- [40] L. Song, W. Ma, Y. Ren, W. Zhou, S. Xie, P. Tan and L. Sun, *Appl. Phys. Lett.*, 2008, **92**, 121905-121908.
- [41] Y. Wang, D. C. Alsmeyer and R. L. McCreery, *Chem. Mater.*, 1990, **2**, 557-563.
- [42] R. Saito, A. Gruneis, G. G. Samsonidze, V. W. Brar, G. Dresselhaus, M. S. Dresselhaus, A. Jorio, L. G. Cancado, C. Fantini, M. A. Pimenta and A. G. S. Filho, *New J. Phys.*, 2003, **5**, 157-171.
- [43] M. Souza, A. Jorio, C. Fantini, B. R. A. Neves, M. A. Pimenta, R. Saito, A. Ismach, E. Joselevich, V. W. Brar, G. Samsonidze, G. Dresselhaus and M. S. Dresselhaus, *Phys. Rev. B*, 2004, **69**, 241403-241406.
- [44] D. Lembke, S. Bertolazzi, and A. Kis. *Acc. Chem. Res.*, 2015, **48**, 100-110.
- [45] N. R. Raravikar, P. Koblinski, A. M. Rao, M. S. Dresselhaus, L. S. Schadler, and P. M. Ajayan. *Phys. Rev. B*, 2002, **66**, 235424.
- [46] D. J. Late, U. Maitra, L. S. Panchakarla, U. V. Waghmare, and C. N. R. Rao. *Journal of Physics: Condensed Matter*, 2011, **23**, 055303.
- [47] K. V. Zakharchenko, M. I. Katsnelson, and A. Fasolino. *Phys. Rev. Lett.*, 2009, **102**, 046808.
- [48] A. Taube, J. Judek, C. Jastrzebski, A. Duzynska, K. Switkowski, and M. Zdrojek. *ACS Appl. Mater. Interfaces*, 2014, **6**, 8959-8963.
- [49] D. J. Late, B. Liu, H. S. S. Matte, C. N. R. Rao, and V. P. Dravid, *Adv. Funct. Mater.*, 2012, **22**, 1894-1905.
- [50] A. C. Gomez, N. Agraït and G. R. Bollinger, *Appl. Phys. Lett.*, 2010, **96**, 213116.
- [51] H. Li, Q. Zhang, C. C. R. Yap, B. K. Tay, T. H. T. Edwin, A. Olivier and D. Baillargeat, *Adv. Funct. Mater.*, 2012, **22**, 1385-1390.
- [52] C. Lee, H. Yan, L. E. Brus, T. F. Heinz, J. Hone and S. Ryu, *ACS Nano*, 2010, **4**, 2695-2700.
- [53] K. Liu, L. Zhang, T. Cao, C. Jin, D. Qiu, Q. Zhou, A. Zettl, P. Yang, S. G. Louie, and F. Wang. *Nat. Commun.*, 2014, **5**, 4966.
- [54] G. C. Constantinescu, and N.D. Hine, *Phys. Rev. B*, 2015, **91**, 195416.
- [55] M. Staiger, R. Gillen, N. Scheuschner, O. Ochedowski, F. Kampmann, M. Schleberger, C. Thomsen, and J. Maultzsch. *Phys. Rev. B*, 2015, **91**, 195419.
- [56] A. R. Beal and W. Y. Liang, *J. Phys. C: Solid State Phys.*, 1976, **9**, 2459-2466.
- [57] C. Sourisseau, F. Cruege and M. Fouassier, *Chem. Phys.*, 1991, **150**, 281-293.
- [58] A. Molina-Sanchez and L. Wirtz, *Phys. Rev. B*, 2011, **84**, 155413-155421.
- [59] E. D. Corro, H. Terrones, A. Elias, C. Fantini, S. Feng, M. A. Nguyen, T. E. Mallouk, M. Terrones and M. A. Pimenta, *ACS Nano*, 2014, **8**, 9629-9635.
- [60] B. Liu, M. Fathi, L. Chen, A. Abbas, Y. Ma, and C. Zhou. *ACS Nano*, 2015, **9**, 6119-6127.
- [61] S. Wang, Y. Rong, Y. Fan, M. Pacios, H. Bhaskaran, K. He, J. H. Warner; *Chem. Mater.*, 2014, **26**, 6371-6379.
- [62] D. J. Late, *ACS Appl. Mater. Interfaces*, 2015, **7**, 5857-5862.
- [63] P. S. Peercy and B. Morosin, *Phys. Rev. B*, 1973, **7**, 2779-2786.

ARTICLE

Journal Name

[64] J. Menendez and M. Cardona, Phys. Rev. B, 1984, **29**,
2051.

Nanoscale Accepted Manuscript

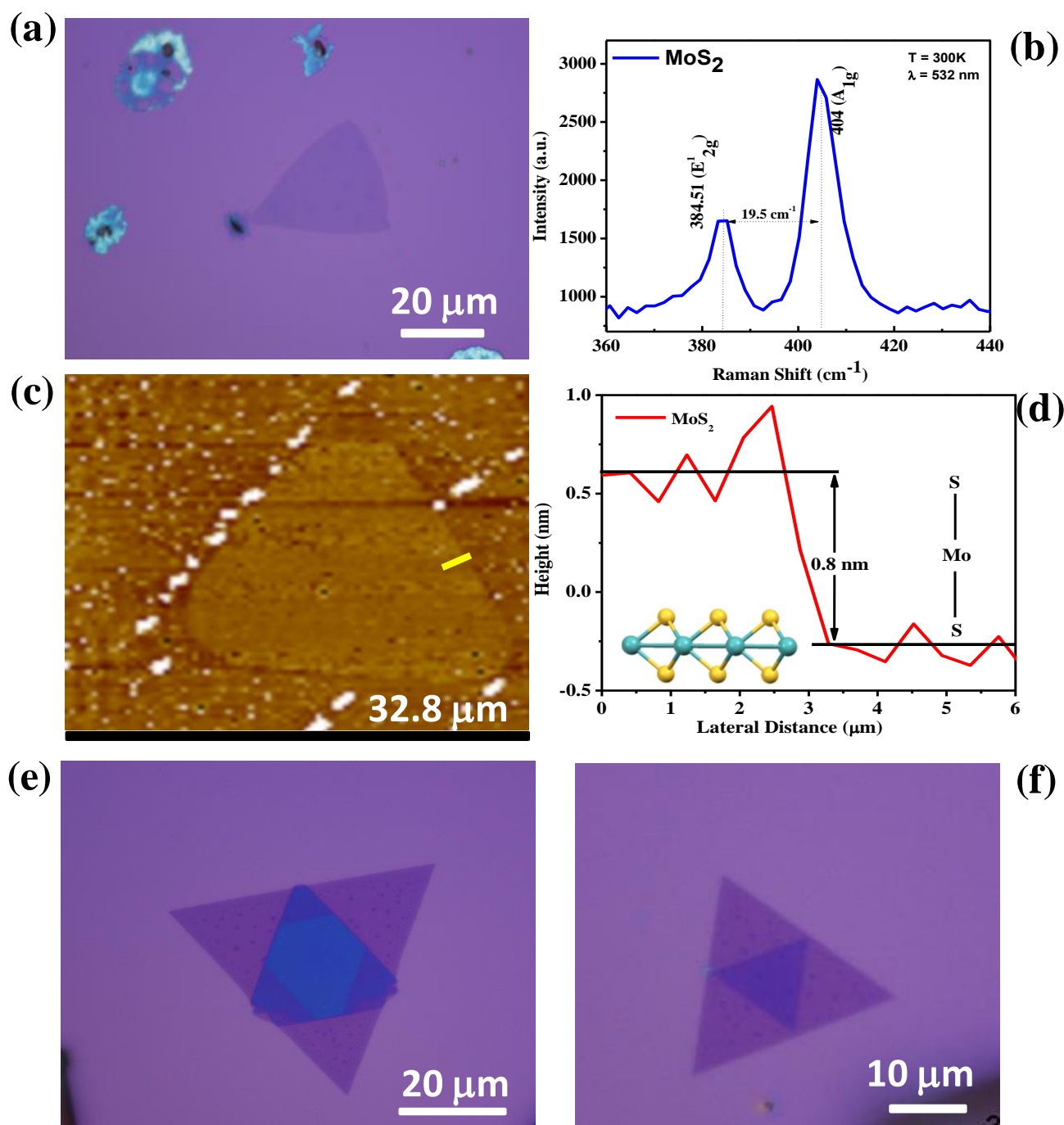
Figure 1:

Figure 1: Chemical vapor deposited single layer MoS₂ (a) Typical optical image, (b) Raman spectrum, (c) AFM image, (d) corresponding AFM height profile and (e – f) Optical images of stacked triangular shape atomically thin MoS₂ layers grown > 750^oC.

Figure 2:

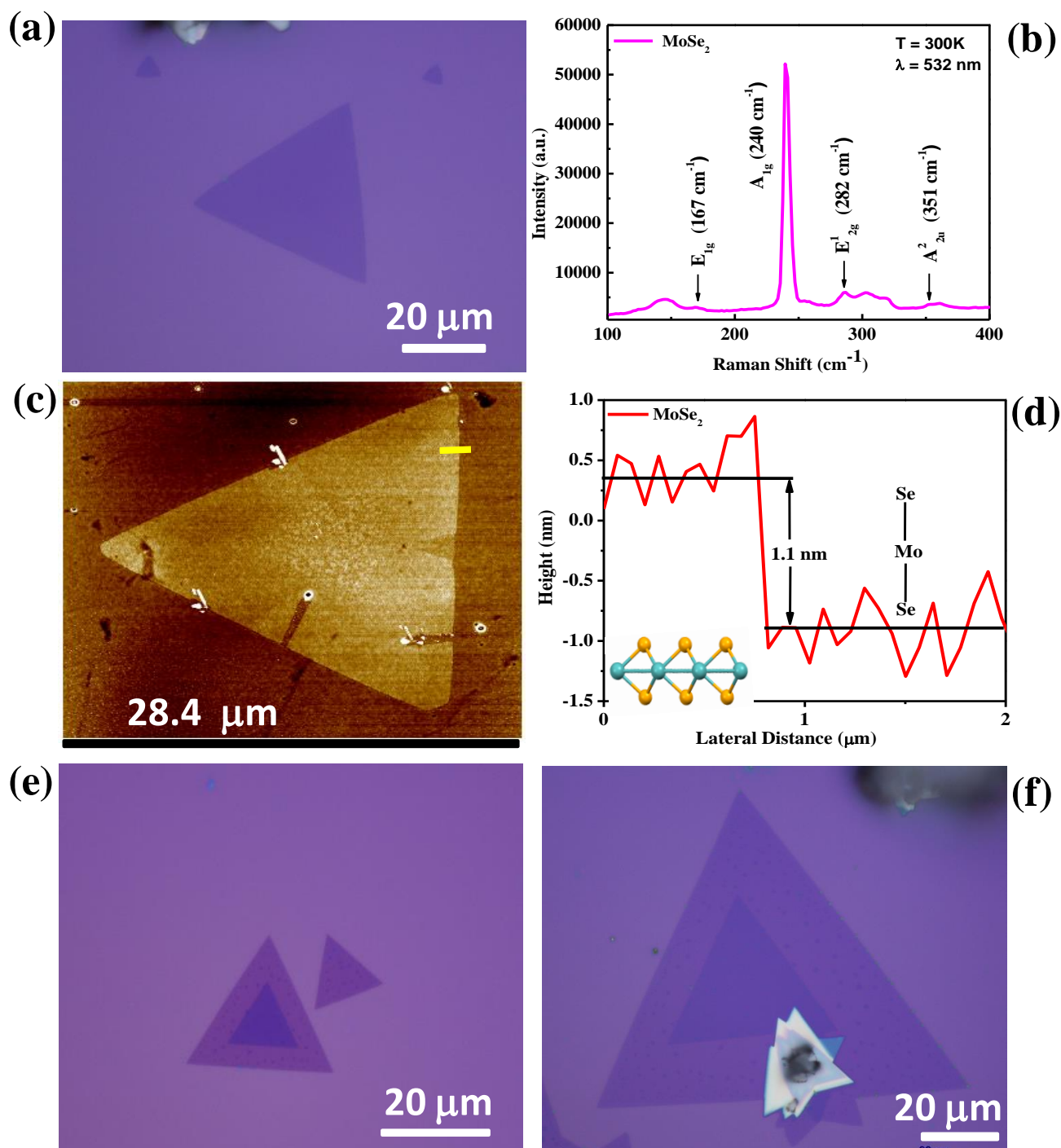


Figure 2: Chemical vapor deposited single layer MoSe₂ (a) Typical optical image, (b) Raman spectrum, (c) AFM image, (d) corresponding AFM height profile and (e – f) Optical images of stacked triangular shape atomically thin MoSe₂ nanosheets grown > 750°C.

Figure 3:

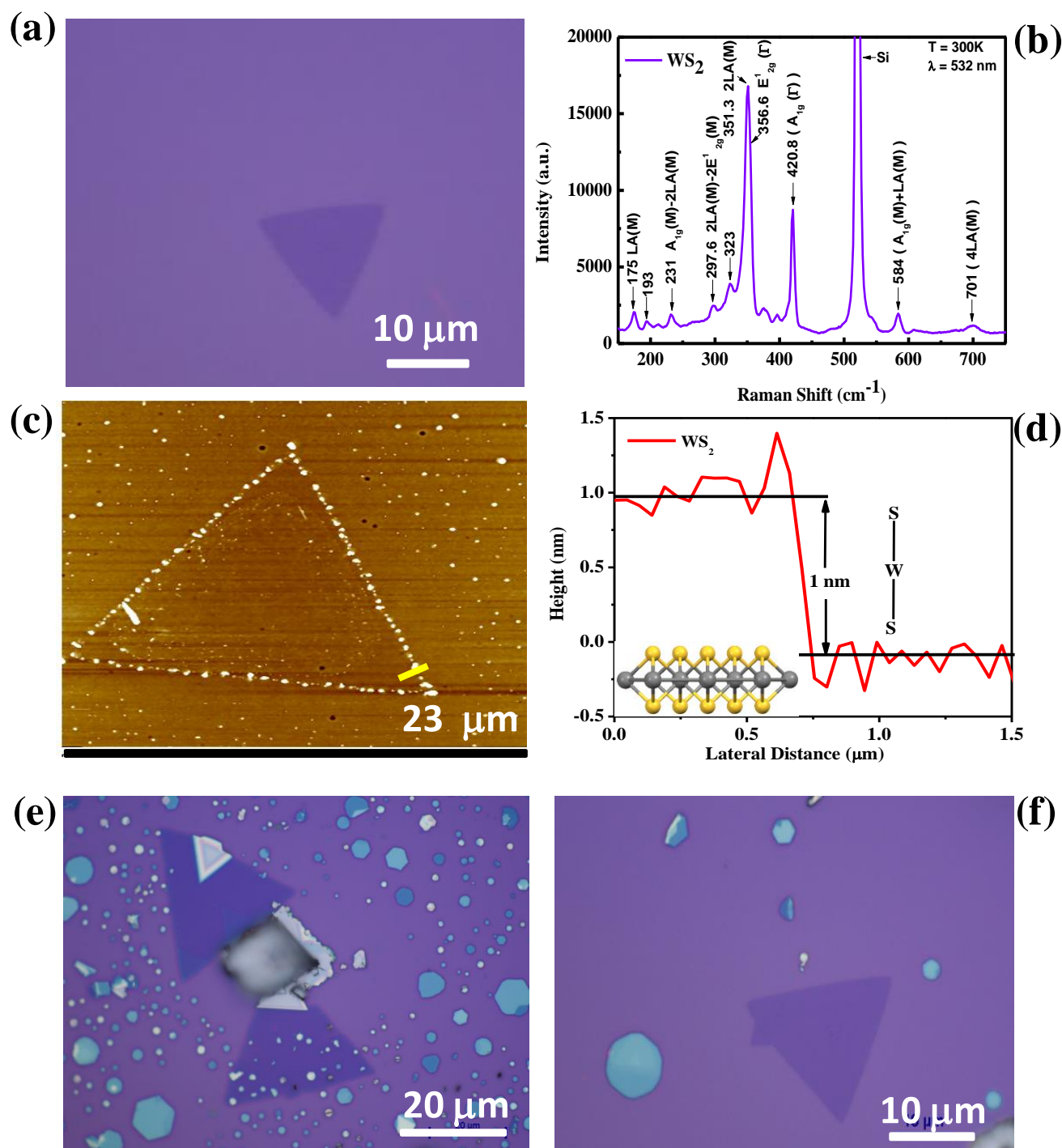


Figure 3: Chemical vapor deposited single layer WS_2 (a) Optical image, (b) Raman spectrum, (c) AFM image, (d) corresponding AFM height profile and (e-f) Optical images of atomically thin hexagonal along with triangular shape of WS_2 nanosheets grown $> 950^\circ\text{C}$.

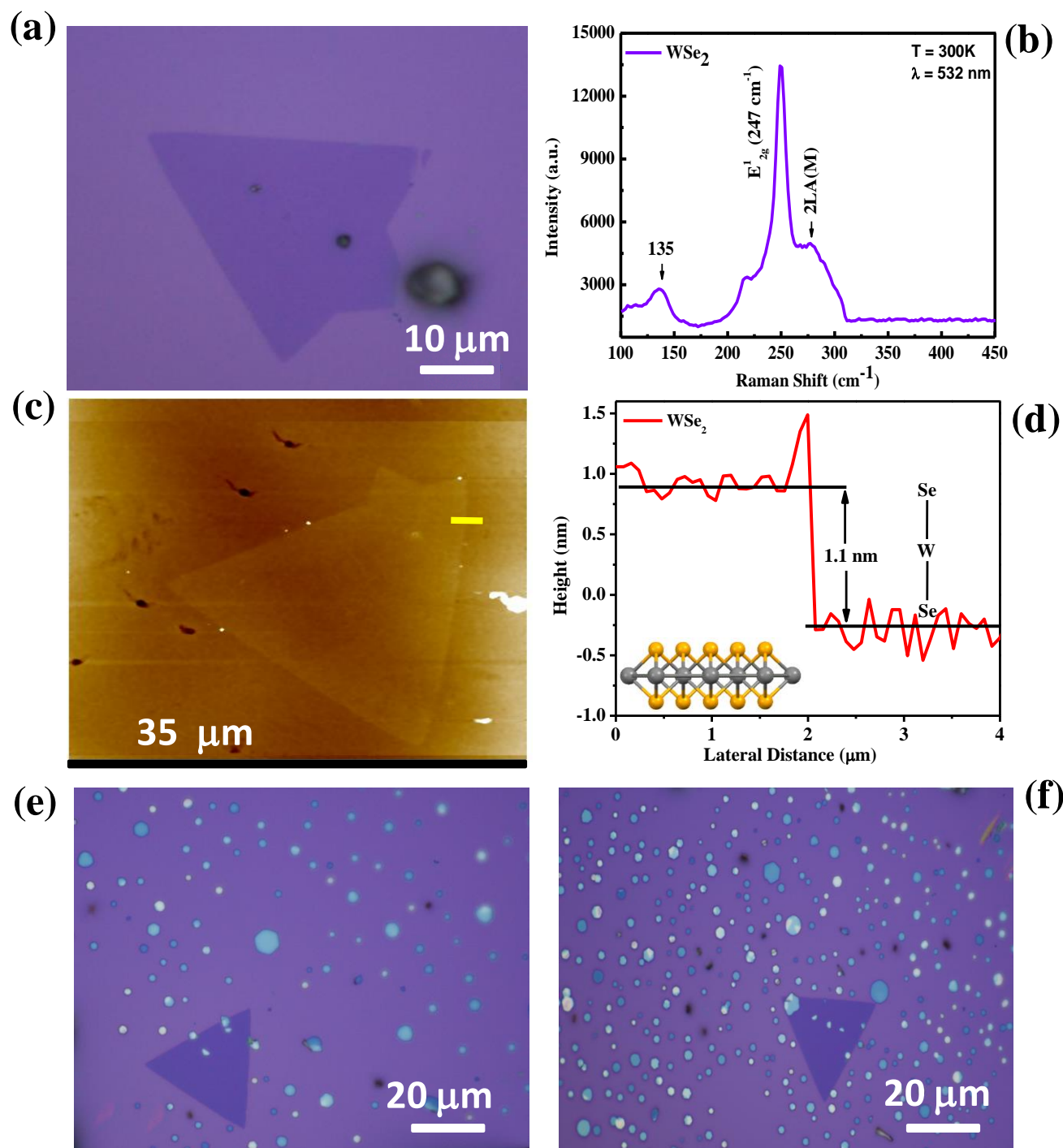
Figure 4:

Figure 4: Chemical vapor deposited single layer WSe_2 (a) Typical optical image, (b) Raman spectrum, (c) AFM image, (d) corresponding AFM height profile and (e-f) Optical images of atomically thin hexagonal along with triangle shape of WSe_2 nanosheets grown $> 950^\circ\text{C}$.

Figure 5:

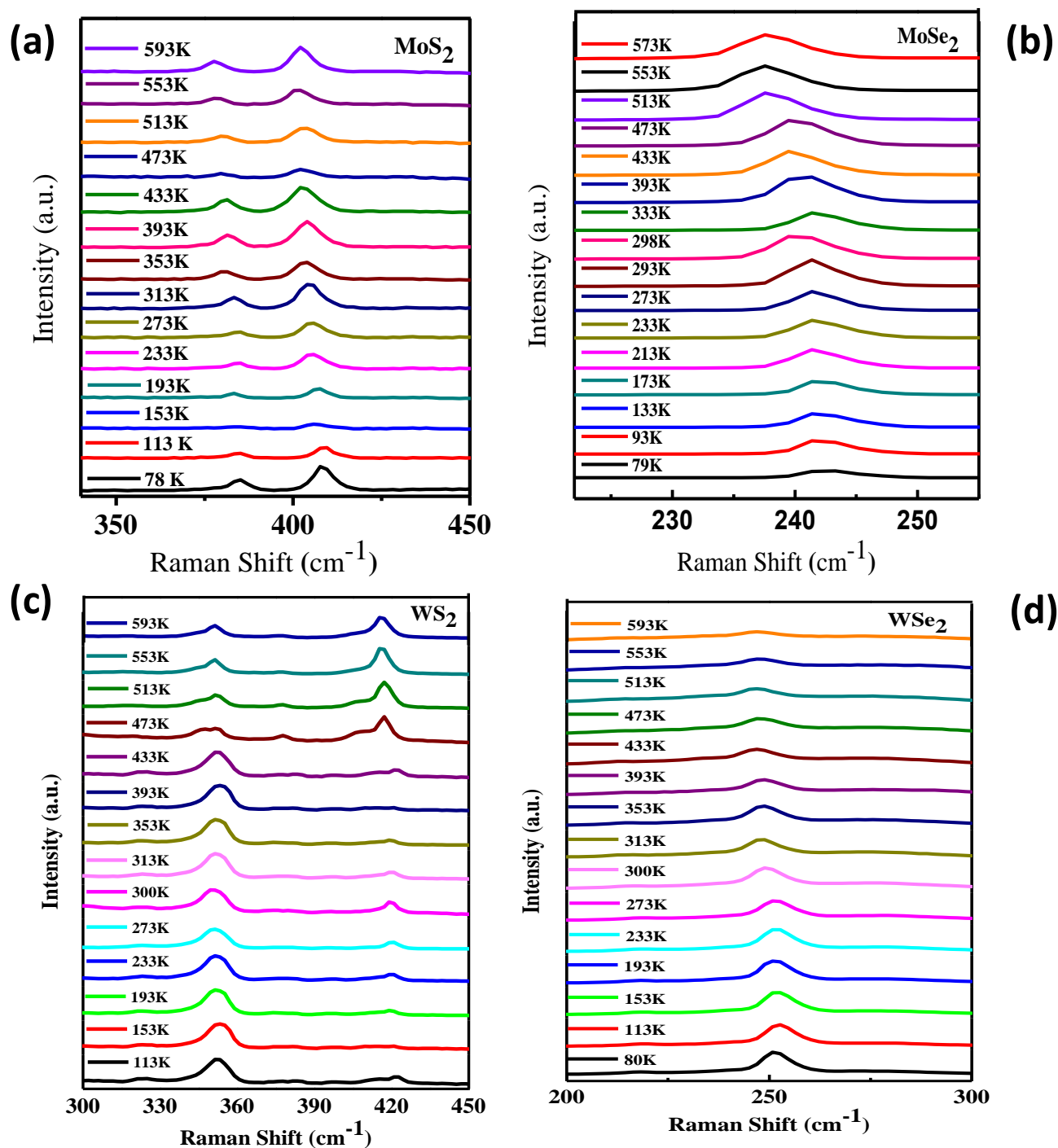


Figure 5: Raman shift as a function of temperature for chemical vapor deposited single layer (a) MoS₂, (b) MoSe₂, (c) WS₂ and (d) WSe₂.

Figure 6:

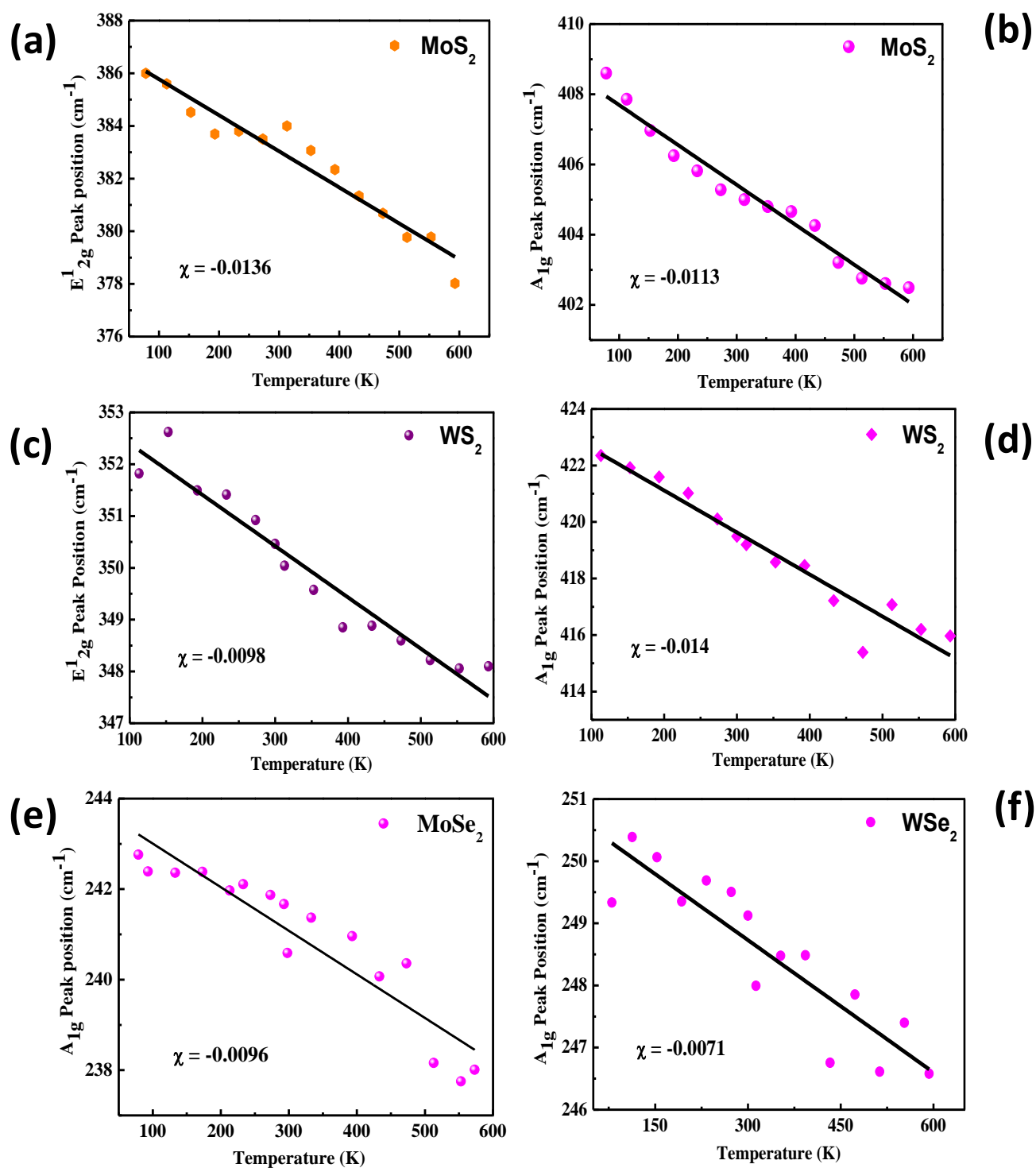


Figure 6: Raman spectra peak position as a function of temperature for chemical vapor deposited monolayer MoS_2 with (a) E_{2g}^1 and (b) A_{1g} mode, WS_2 (c) E_{2g}^1 and (d) A_{1g} mode. For MoSe_2 (e) A_{1g} mode and for WSe_2 (f) A_{1g} mode respectively.

Table 1:

Monolayer TMDCs	Raman Modes	Observed Temp. coefficient χ ($\text{cm}^{-1}\text{K}^{-1}$)	$\Delta\omega$ (cm^{-1})
MoS ₂	E _{2g} ¹	-0.0136	8
	A _{1g}	-0.0113	6.11
MoSe ₂	A _{1g}	-0.0096	4.75
WS ₂	E _{2g} ¹	-0.0098	4.51
	A _{1g}	-0.014	6.43
WSe ₂	A _{1g}	-0.0071	3.81

Table 1: The temperature coefficients and frequency difference for chemical vapor deposited single-layer TMDCs.